Supporting Information for Mónica M. Lozano, Zhao Liu, Eva Sunnick, Andreas Janshoff, Krishna Kumar, and Steven G. Boxer. *Co-localization of the Ganglioside G_{M1} and Cholesterol Detected by Secondary Ion Mass Spectrometry*.

Table of Contents

Synthesis of isotopically labeled and fluorinated membrane components for nanoSIMS imaging

Biosynthesis of ^{13}C-labeled cholesterol

Materials

Hep G2 cells were a gift from the Sarnow Laboratory in the Department of Microbiology and Immunology at Stanford University School of Medicine. Glucose-free Dulbecco's modified Eagle's medium (DMEM), fetal bovine serum (FBS), 100X penicillin-streptomycin (Pen-Strep), and 100X Non-Essential Amino Acids (NEAA) were from Invitrogen. Analytical grade chloroform and methanol, HPLC-grade hexanes, isopropanol, and glacial acetic acid and anhydrous ethyl ether were from Fisher Scientific Inc. Sodium [1,2-^{13}C]-acetate (99% abundance) was from Cambridge Isotope Laboratories.

Cell culturing

The human hepatobalstomama Hep G2 cells were first cultured at 37^{o}C and 5% CO_2 in 60mm dishes in glucose-free Dulbecco's modified Eagle's medium (DMEM) with 1% Pen-Strep (v/v) and 1% NEAA (v/v) supplemented with 10% fetal bovine serum (FBS) until 100% confluence, and then transferred to 60mm culture dishes at an initial cell density of $2x10^6$ cells/dish and switched to media that is instead supplemented with 2mM sodium [1,2-^{13}C]-acetate (Cambridge Isotope Laboratories, 99% abundance) and 0.5g delipidated FBS. The choice of cell density was a balance between optimum sodium [1,2-^{13}C]-acetate content per $1x10^6$ cells without significantly changing the pH of the media. Media was exchanged twice a day for 7 days. In an effort to optimize ^{13}C-enrichment, it was necessary to remove ^{12}C-cholesterol sources originating from media supplements. It appeared that the main source of residual ^{12}C-cholesterol came from the serum, therefore delipidated serum was prepared as described by Rothblat et al (1976).[1] Briefly, 50mL FBS was added to 450mL ice-cold 1:1 acetone:ethanol, incubated in ice for 4 hrs and swirled every 30min. The delipidated serum protein was collected on 5 separate 9.0cm Whatman #1 papers by suction through a Buchner funnel and washed with 125mL pre-cooled ethyl ether. Suction was maintained until the protein became flaky and was then removed from the paper and stored in a vacuum desiccator overnight. The dried serum protein (~0.5g) was solubilized in 500mL cell culturing media.

Total Lipid Extraction.

Extraction and separation of lipids from $30x10^6$ Hep G2 cells was performed using a modified microprocedure based on the Folch et al.[2] and Suzuki[3] extraction methods that was easily applied to micromolar quantities of lipids.[4] Extraction and separation of lipids from Hep G2 cells grown in 60mm tissue culture dishes at a cell density of $2x10^6$ cells/dish were performed as described by Wersto and Druyan (1982).[5] The media from the culture dishes was aspirated and cells were washed with ice-cold phosphate buffered saline (PBS, pH 7.2) to remove trace media. The PBS was aspirated and replaced with fresh ice-cold PBS. Using a tissue scraper, the attached cells were removed and transferred to a centrifuge tube. The cell suspension was centrifuged in an IEC CL30R centrifuge (Thermo Electron Corporation) at 1000G for 15min at 4°C. The supernatant was aspirated and the cell pellet was resuspended in 1mL ice-cold PBS. The cell suspension was transferred to a 15mL glass centrifuge tube with a Teflon-lined screw cap (Kontes) and centrifuged in an RC 5B Plus centrifuge (Sorvall) at 4500RPM for 10min at 4°C for this and all subsequent spins. The supernatant was aspirated and the cell pellet was resuspended in 3mL 2:1 $CHCl_3$:CH_3OH and transferred to a tissue grinder (Duall, size 22, Kontes). The cells were ground for 2min and vortexed for 1min seven times. The lysate was transferred to and centrifuged in a 15mL glass centrifuge tube. The supernatant was collected and transferred to a 15mL glass centrifuge tube and stored in ice while the pellet was resuspended in 3mL 1:1 $CHCl_3$:CH_3OH and transferred to the tissue grinder. The cells were ground and vortexed as previously described. The lysate was transferred to and centrifuged in a 15mL glass centrifuge tube. The extract was collected and combined with the extract from the previous step and stored in ice while the cell pellet was resuspended in 3mL 1:2 $CHCl_3$:CH_3OH and transferred to the tissue grinder. The cells were ground and vortexed for a last time as previously described. The lysate was transferred to and centrifuged in a 15mL glass centrifuge tube. The supernatant was collected and combined with the extract from the previous steps and stored in ice while the cell pellet was resuspended in 3mL 2:1 $CHCl_3$:CH_3OH and centrifuged. Again

the supernatant was combined with previous extracts. 3mL chloroform were added to the combined extracts to make the mixture 2:1 $CHCl_3$:CH_3OH and 2.2mL 0.9% w/v NaCl in water were added. The tube was vortexed vigorously and centrifuged. The upper phase was removed and discarded and an additional 1.8mL 0.9% w/v NaCl in water was added. The tube was vortexed vigorously and centrifuged. The upper phase was removed and discarded. The solvent was then evaporated by a gentle stream of nitrogen gas over a heating plate at 40°C and placed in a vacuum desiccator overnight. The dried total lipid extract was dissolved in 100µL 2:1 $CHCl_3$:CH_3OH.

Separation of cholesterol by HPLC.

Lipid classes were first separated as described by Wersto and Druyan (1982).[5] Briefly, 0.3g of activated (100°C for 12hrs) silicic acid was placed in a 15mL conical glass centrifuge tube, 5mL CH_3OH was added and the solution was vortexed. The slurry was then transferred to a 5¾" Pasteur pipette pre-plugged with glass wool. The silicic acid column was washed sequentially with 5mL $CHCl_3$, CH_3OH, and $CHCl_3$ allowing the last wash to drain 3mm from the top of the column. Lipid extract was added to the column. The neutral lipids and cholesterol fraction was eluted by adding 6mL $CHCl_3$ and eluate was collected in a 15mL conical glass tube. Phospholipids were eluted by adding 6mL CH_3OH and eluate was collected in another 15mL conical glass tube. Solvent from both eluates was evaporated by using a gentle stream of nitrogen gas over a heating plate at 40°C. Neutral lipids and cholesterol fraction was resuspended in 300µL hexane:isopropanol:glacial acetic acid 100:2:0.02 for HPLC separation.

Cholesterol was separated from neutral lipids by an LC-20AT Prominence Liquid Chromatographer equipped with an SPD-10A Shimadzu UV-VS detector operated at 206nm and an FRC-10A Shimadzu fraction collector. The LC column is a 250x10mmID Duragel G 5µm C4 (Peeke Scientific). The mobile phase was hexane:isopropanol:glacial acetic acid 100:2:0.02 at a flow rate of 2.5mL/min. A standard cholesterol peak emerged at 8.5min. The amount of cholesterol extract was determined from a calibration curve to be ~16nmol / $1x10^6$ cells.

Detection of cholesterol by MS

The isotopic analysis of ^{13}C-cholesterol was analyzed by loop injection (40µL) on a ThermoFinnigan LCQ ion trap mass spectrometer. The MS was operated in +APCI (atmospheric pressure chemical ionization) mode, with CH_3OH as the carrier solvent at 200µL/min (see **Figure S1**).

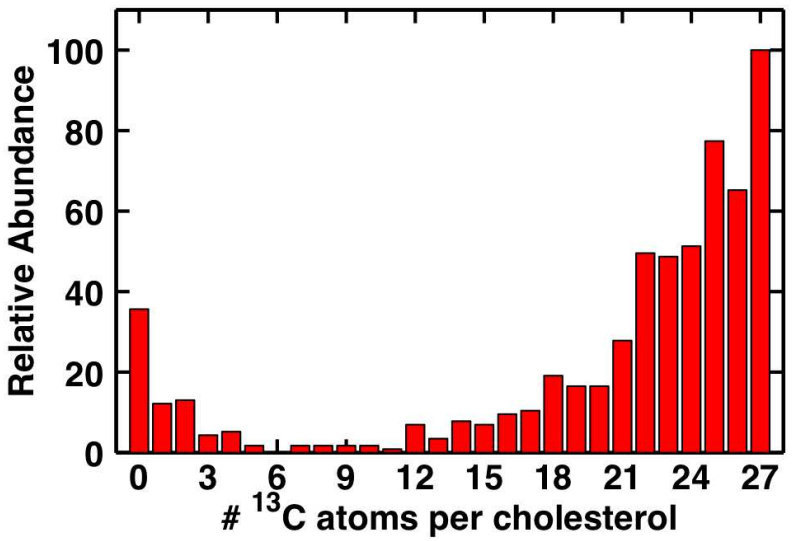

Figure S1. Mass spectra of ^{13}C-labeled cholesterol isotopomer distribution.

Synthesis of ^{15}N-labeled DOPC

The synthesis of ^{15}N-DOPC was performed following the protocol described by Kraft et al.[6] for the synthesis of ^{15}N-DLPC. Briefly, anhydrous pyridine (20mL) was added to a flame-dried 50mL round bottom flask charged with ^{15}N-choline chloride (515mg, 3.662mmol, Sigma Aldrich), 1,2-dioleoyl-sn-glycero-3-phosphate (264mg, 0.366mmol, Avanti Lipids) and a stir bar. Trichloroacetonitrile (3.47mL) was slowly added to the flask, and the solution was placed in a 60^{o}C oil bath and stirred overnight. The solution was cooled, filtered to remove the precipitate, and concentrated via rotary evaporation under reduced pressure. To completely remove the pyridine, the brown residue was dissolved in 40mL *CH3OH*:$CHCl_3$ (1:1) and concentrated via rotary evaporation under reduced pressure. Column chromatography on IWT TMD-8 ion exchange resin (50% tetrahydrofuran in water) yielded the product as a light brown wax. Column chromatography on silica gel ($CHCl_3$:CH_3OH:H_20 65:25:4) produced the product as a beige wax that was re-purified by column chromatography on octadecyl-functionalized silica gel ($CHCl_3$:CH_3OH 5:95), yielding the pure phosphocholine (92.9mg, 32.2% yield) as a white wax.

Synthesis of 18-F-G_{M1}

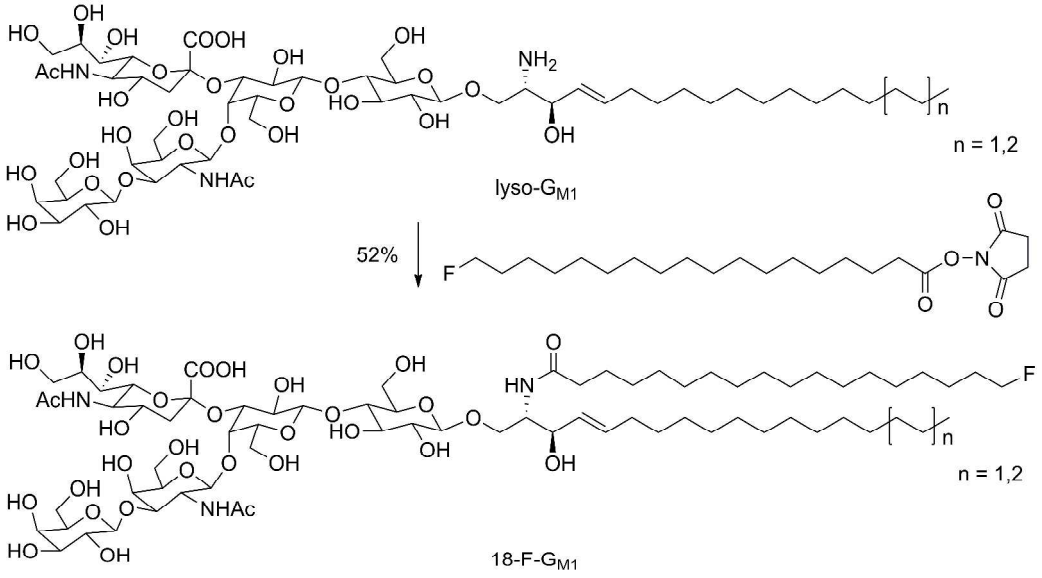

Scheme S1. Synthetic scheme of 18-F-GM1.

To a round bottom flask charged with a suspension of the NHS ester of 18-fluorostearate (35 mg, 87 µmol) and lysoG$_{M1}$ (60 mg, 48 µmol) was added 10 µl diisopropylethyl amine (58 µmol). The mixture was stirred at rt for 12 h. Solvent was removed *in vacuo* and the resulting residue was subjected to flash column chromatography ($CHCl_3$-MeOH-H_2O, 60:40:5, v/v/v) to give 18-F-G$_{M1}$ as a white powder (38 mg, 52%).

^{1}H NMR (CDCl3, 500 MHz) *δ* 5.68 (dt, 1H), 5.44 (dd, 1H), 4.92 (d, 1H), 4.45 (d, 1H), 4.41 (d, 1H), 4.35 (t, 1H), 4.29 (d, 1H), 4.19 (d, 1H), 4.15 (s, 1H), 4.07 (t, 1H), 4.00 (s, 2H), 3.97 (m, 1H), 3.87 (m, 5H), 3.76 (m, 2H), 3.69 (m, 6H), 3.53 (m, 5H), 3.40 (m, 3H), 3.27 (s, 1H), 2.74 (m, 1H), 2.17 (t, 1H), 2.00 (s, 3H), 1.99 (s, 3H), 1.91 (t, 1H), 1.69 (m, 2H), 1.57 (b, 2H), 1.38 (b, 3H), 1.29 (b, 35H), 0.90 (t, 3H)

^{19}F NMR ($CDCl_3$, 470 MHz) δ 218.4 (m)

HRMS ((+)ESI): (18-F-G$_{M1}$, n = 1) *m*/*z* [$C_{73}H_{130}FN_3O_{31}$+Na]$^+$ *calcd*: 1586.8565, *found*: 1586.8460; (18-F-G$_{M1}$, n = 2) *m*/*z* [$C_{75}H_{134}FN_3O_{31}$+Na]$^+$ *calcd*: 1614.8883*, found*: 1614.8820.

Interrogating the effect of fluorination of G_{M1} in cell and model membranes

Calcium Signaling Assay

Materials

Human T cell leukemia Jurkat clone E6.1 (ATCC TIB-152) were from American Type Culture Collection (ATCC). Cholera toxin B subunit (CTB) was from Sigma-Aldrich. Fura-2 acetoxymethyl ester (Fura-2/AM) was from AXXORA. Anti-CTB antibody was from Meridian Life Science. Ganglioside G_{M1} was isolated and purified from bovine brain tissue. Other common reagents were from Sigma-Aldrich.

Cell culturing

Jurkat T cells were cultured in RPMI 1640 medium supplemented with 10% FBS (v/v) and 1% penicillin (v/v). Cells were incubated at 37 °C for 24 h and the medium was then replaced with one supplemented with 25 μM ganglioside G_{M1} or 18-F-G_{M1} for 2 h followed by incubation with 250 ng/mL CTB for 1 h after washing 3 x 2 mL with 1X PBS ($-Ca^{2+}$, $-Mg^{2+}$).

Ca^{2+} signaling

Jurkat T cells were washed 3 x 2 mL with 50 mM HEPES buffer (pH 7.2, supplemented with 120 mM NaCl, 1 mM $CaCl_2$, 0.5 mM $MgCl_2$, 5 mM KCl, 1 mM Na_2HPO_4, and 1 mg/mL of glucose), incubated in 400 μL fura-2/AM (5 mM in HEPES buffer) for 20 min, and then treated with 7 mL HEPES buffer for 20 min. Cells were washed once with HEPES (2 mL) and then re-suspended in 2 mL of buffer. Cuvettes containing cells were equilibrated at 37 °C for 5 min and the fluorescence was measured with λ_{ex} at 340 and 380 nm and λ_{em} at 510 nm (10 nm slit widths). Ca^{2+} uptake by cells was triggered by adding anti-CTB antibody (40 μg/mL), and monitored at 37 °C for 10 min.

18-F-G_{M1} induces calcium signaling in Jurkat cells

It is important to demonstrate that 18-F-G_{M1} behaves the same as G_{M1} *in vivo*. G_{M1} is involved in a variety of cellular pathways including calcium signaling. Gouy et al. observed an increase in the cytosolic [Ca^{2+}] in Jurkat cells that display G_{M1} on their surfaces, triggered by treatment with CTB followed by addition of an anti-CTB antibody.[7] In our experiment, Jurkat cells were used to evaluate the ability of 18-F-G_{M1} to induce calcium signaling. The cytosolic Ca^{2+} concentration was monitored by comparing the ratio of Fura-2 fluorescence excitation intensities at 340 and 380 nm (R_{340}/R_{380}) where an increase in this ratio is indicative of elevation of Ca^{2+} bound Fura-2 in the cytosol. Upon incubation with native G_{M1} (25 μM), the Ca^{2+} influx was significantly enhanced (**Figure S2**, blue) compared to that in cells that received no G_{M1} treatment (**Figure S2**, black). We found 18-F-G_{M1} at 25 μM behaves similarly to native G_{M1} (**Figure S2**, red) and is competent in promoting Ca^{2+} uptake in cells to the same extent as native G_{M1}.

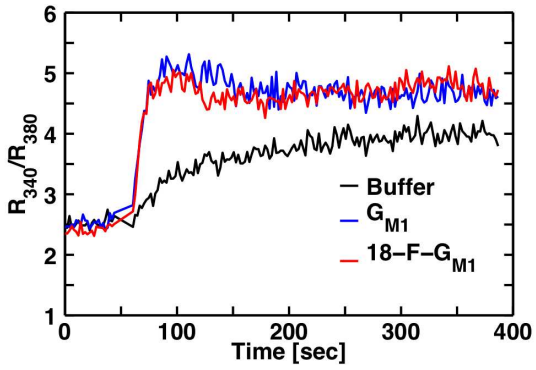

Figure S2. G_{M1} and 18-F-G_{M1} are indistinguishable in calcium influx induced by G_{M1} or 18-F-G_{M1} in Jurkat cells. Jurkat cells were incubated with buffer (black line), 25 μM native G_{M1} (blue), or 25 μM 18-F-G_{M1} (red) followed by binding of CTB (250 ng/mL), fura-2/AM (5mM), and anti-B antibody (40 μg/mL). The cytosolic calcium concentration was monitored from changes

in fluorescence intensity (FI) of fura-2 (at λ_{ex}=340 and 380 both at λ_{em}=510) and was measured by taking the ratio of $R_{340}=FI_{340}/FI_{510}$ to $R_{380}=FI_{380}/FI_{510}$ (i.e. R_{340}/R_{380}) over time.

FACS assay

Materials

CHO-K1 cells (ATCC CCL-61) were from American Type Culture Collection (ATCC). Fluorescein isothiocyanate (FITC)-labeled cholera toxin B subunit (FITC-CTB) were from Sigma-Aldrich. The cell growth medium and buffers were from Cancer Center, Tufts Medical Center, and Invitrogen. Ganglioside G_{M1} was isolated and purified from bovine brain tissue.

Sample Preparation

CHO-K1 cells were first cultured in Ham's F12 medium with 10% FBS (v/v) and 1% penicillin (v/v) at 37 °C for 12 h in 6-well plates at a density of $1x10^6$ cells/well. This allowed adhesion of the cells at the bottom of the well. The cells were then switched to fresh media supplemented with native G_{M1} or 18-F-G_{M1} and incubated at 37 °C for 2 h. The cells were then washed 3 x 2 mL with fresh media followed by treatment with FITC-CTB (250 ng/mL) in fresh media for 1 h. After washing 3 x 2 mL with 1X PBS ($-Ca^{2+}$, $-Mg^{2+}$), cells were fixed with 5% paraformaldehyde and analyzed by flow cytometry (BD Bioscience FACSCalibur, San Jose, CA).

Incorporation of 18-F-G_{M1} on CHO-K1 cells is concentration dependent

G_{M1} serves as the receptor for cholera toxin that contains an "A" subunit and a pentavalent "B" subunit. Crystallographic studies have shown that the B subunit of cholera toxin binds to the oligosaccharide moiety of GM1, exposed on the outer surface of cell membranes. Exogenously delivered G_{M1} is incorporated on the outer leaflet of plasma membranes and is recognized by cholera toxin. We further demonstrate using FACS that the fluorine atom distally located in the terminus of the stearic acid chain does not influence cholera toxin B binding. We investigated the incorporation of 18-F-G_{M1} on CHO-K1 cells that are devoid of G_{M1}. CHO-K1 cells incubated with 18-F-G_{M1} were analyzed by flow cytometry after staining with FITC-CTB. The fluorinated G_{M1} on cell surfaces is recognized by FITC-CTB, as judged by the fluorescence emanating from the cells. The fluorescence intensity in flow cytometry is also indicative that the amount of FITC-CTB staining in cells incubated with 18-F-G_{M1} (**Figure S3**, red, orange, and yellow) is similar to those cells containing native GM1 (**Figure S3**, dark blue, blue, and light blue) and both more fluorescently intense than cells without exogenously delivered GM1 (**Figure S3**, black). Since the CTB binds to the pentasaccharide epitope of G_{M1}, the single fluorine atom in 18-F-G_{M1} that is distally located on the terminus of the fatty acid chain does not seem to influence binding. The incorporation of 18-F-G_{M1} on CHO-K1 cells was shown to be concentration dependant in the 0.2 to 5 μM range in culture media (**Figure S3**).

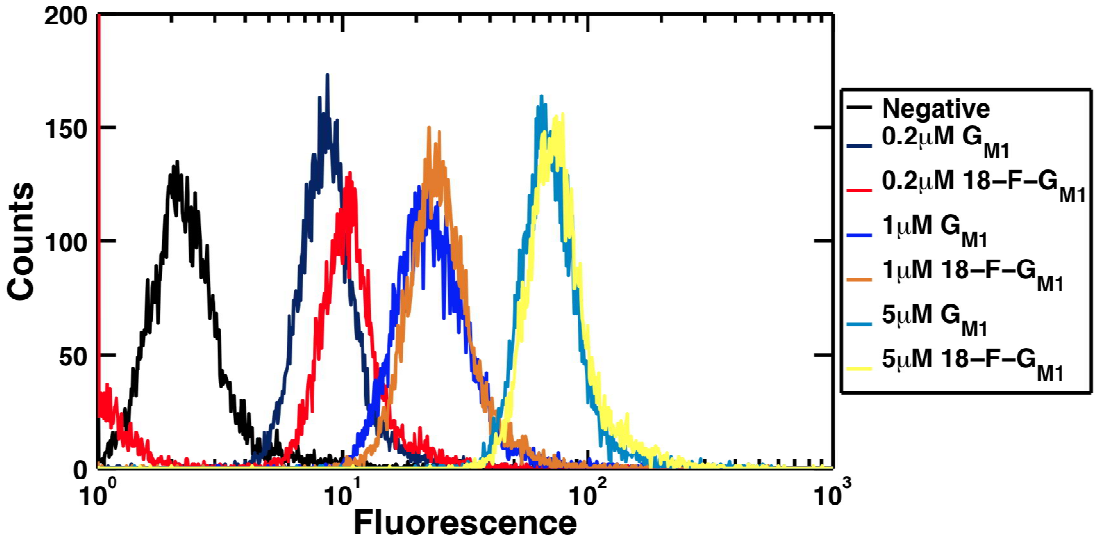

Figure S3. Flow cytometry histograms of FITC-CTB labeled native or fluorinated GM1 exogenously delivered to the plasma membrane of CHO-K1 cells. Negtive control (black); 0.2 μM (dark blue), 1.5 μM (blue), and 5 μM (light blue) native G_{M1}; 0.2 μM (red), 1.5 μM (orange), and 5 μM (yellow) 18-^{19}F-GM1. Sample size = 10,000 counts.

Atomic Force Microscopy imaging

Materials

Ganglioside G_{M1} was isolated and purified from bovine brain tissue. 1-palmitoyl-2-oleoyl-sn-glycero-3-phosphocholine (POPC) and 1,2-dipalmitoyl-sn-glycero-3-phosphocholine (DPPC) were from Sigma-Aldrich.

Preparation of supported lipid bilayers

Supported lipid bilayers were prepared by fusion of small unilamellar vesicles (SUVs) to solid mica substrates. Briefly, a 1:1 DPPC:POPC with 1mol% native G_{M1} or 18-F-G_{M1} lipid mixture was dissolved in chloroform followed by evaporation of the solvent by a gentle stream of Ar. The dried lipid film was then hydrated with Tris Buffer (pH 7.4) to a final 1 mM lipid concentration and incubated for 30min at 55^{o}C with occasional gentle vortexing to afford a clear solution. SUVs were prepared by tip sonicating the hydrated lipid mixture for 30min at RT. Solid supported lipid bilayers were prepared by adding 0.5 mL Tris buffer (pH 7.4) and 15 μL of a 0.1 M $CaCl_2$ solution to a freshly cleaved mica surface followed by the addition of 125μL SUV solution and allowed to equilibrate overnight at room temperature. Prior to AFM imaging, the samples were incubated at 55 ºC for 30 min and then cooled to RT at ambient conditions. The supported lipid bilayer samples were then rinsed 3 × 2 mL with Tris buffer (pH7.4) to remove excess SUVs and 1 mL of the same buffer was added for AFM imaging.

Atomic force microscopy

AFM was performed in aqueous solutions using a NanoWizard II® (JPK Instruments AG, Berlin, Germany) equipped with a fluid cell, using a MSCT-Au (Veeco, Santa Barbara, CA, USA) with a nominal spring constant of 0.1 N/m. The acquired data were processed using Gwyddion (JPK Instruments AG).

Phase separation of 18-F-G_{M1} in solid supported lipid bilayers by AFM

It is also important to demonstrate that 18-F-G_{M1} displays the same behavior as native G_{M1} in phase-separated supported lipid bilayers (SLBs) analyzed by AFM. SLBs were formed by fusion of SUVs composed of DPPC/POPC (1:1) with 1 mol% 18-F-G_{M1} onto mica surfaces, somewhat different from the samples used for NanoSIMS imaging. AFM imaging reveals gel/L_d phase coexistence at approximately 1:1 ratio (**Figure S4A**). Analysis of the height profiles indicate accumulation of 18-F-G_{M1} within the gel and L_d phases into ~10nm diameter regions that are ~0.5nm higher than the surrounding phase (see arrows in Profiles 1 and 2, **Figure 4A**). The observations reported here with 18-F-G_{M1} are consistent with the phase behavior of native G_{M1} in lipid bilayers (see arrows in Profiles 1 and 3, **Figure S4B**). The thickness of the gel/L_d phases of the fully hydrated lipid bilayers containing either native G_{M1} or 18-F-G_{M1} was determined to be 4.9nm/3.5nm and 6.5nm/4.9nm, respectively. These values were obtained by measuring the height difference between the mica substrate (dark regions) and the gel/L_d phases of the lipid bilayer (see Profile 3, **Figure S4A** and Profile 2, **Figure S4B**) and are consistent with reported literature values.[8]

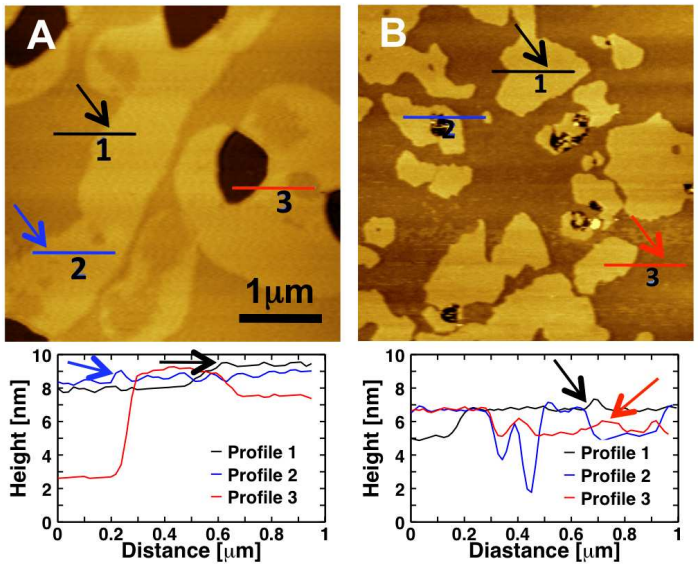

Figure S4. AFM images of DPPC/POPC (1:1) mixture with 1mol% native G_{M1} (A) or 18-F-G_{M1} (B). The higher domains (brighter regions) are gel phases surrounded by a slightly lower, L_d phase. The lowest regions (dark regions) correspond to the mica substrate and indicate holes or defects in the lipid bilayer. Each profile curve represents the corresponding height scanning line in the image. Arrows correspond to the accumulation of native G_{M1} or 18-F-G_{M1} based on height differences.

Supplementary Figures

Fluorescence microscopy imaging

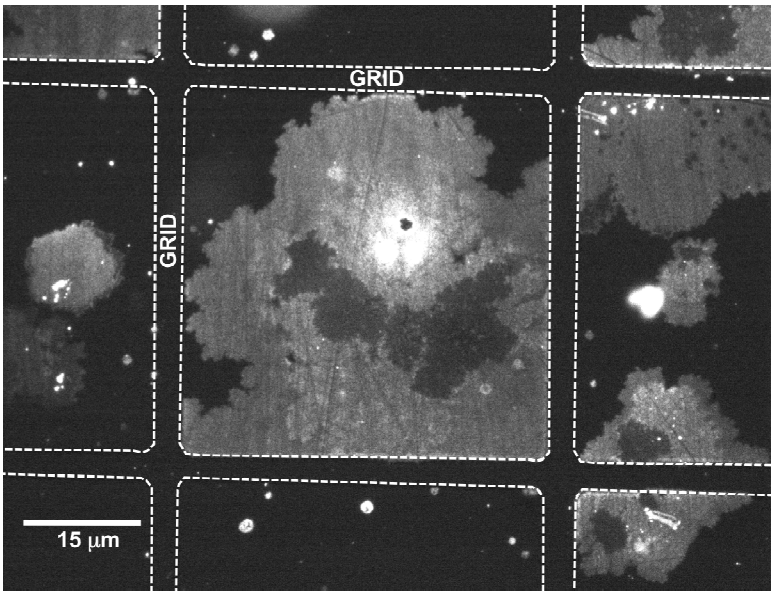

Figure S5. Fluorescence micrograph of a hydrated, ^{2}H-SM:^{15}N-DOPC:^{13}C-Cholesterol:18-F-G_{M1}-containing lipid bilayer on an SiO_2/Si substrate within 50μm x 50μm chrome grids (width = 5μm, height ~5nm) followed thermal treatment highlighting the differential partitioning of TR-DHPE into a dark, liquid ordered phase surrounded by a bright, liquid disordered phase. The effect of the lipid bilayer edge appears highlighted by intermediate fluorescence intensity.

NanoSIMS High Mass Resolving Spectra

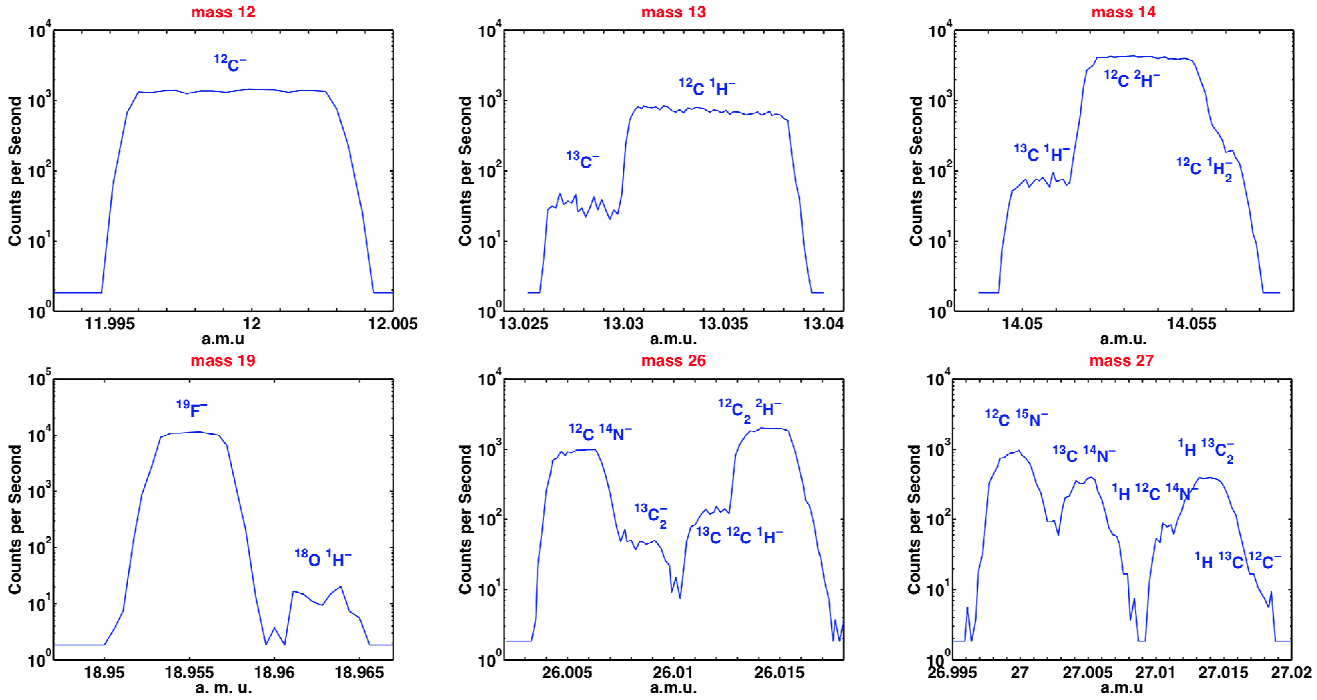

Figure S6. NanoSIMS High Mass Resolving Spectra. Mass spectra (secondary ion counts per second vs. atomic mass) obtained using the NanoSIMS 50L at Stanford University set at high mass resolving power (MRP) for species at masses 12 (MRP~1,700), 13 (MRP~1,700), 14 (MRP~8,900), 19 (MRP~7,400), 26 (MRP~3000), and 27 (MRP~13,100) showing the ability to differentiate species at similar masses and determine the isotopic enrichment of the sample.

Correction to $^{12}C^2H^-$ ion counts

The measured $^{12}C^2H^-$ ion counts were corrected from contributions from isobaric interferences $^{13}C^1H^-$ and/or $^{12}C^1H_2^-$ by subtracting the uncorrected measured ratio from a blank oxidized silicon substrate (r_{blank}) from the uncorrected measured ratio for all samples (r^*).

A	$^{12}C^2H^-$ ion counts
B	$^{12}C^-$ ion counts
X	Contributing counts from $^{13}C^1H^-$ and/or $^{12}C^1H_2^-$ ion species to $^{12}C^2H^-$
$r^* = \left[\frac{A+X}{B}\right]^*$	Measured (uncorrected) ion ratio
$r_{blank} = \left[\frac{A+X}{B}\right]_{blank} = 7.7x10^{-2}$	Measured (uncorrected) ion ratio from an oxidized silicon substrate
$r = r^* - r_{blank}$	Corrected ion ratio

Calibration Curves from Standard Samples

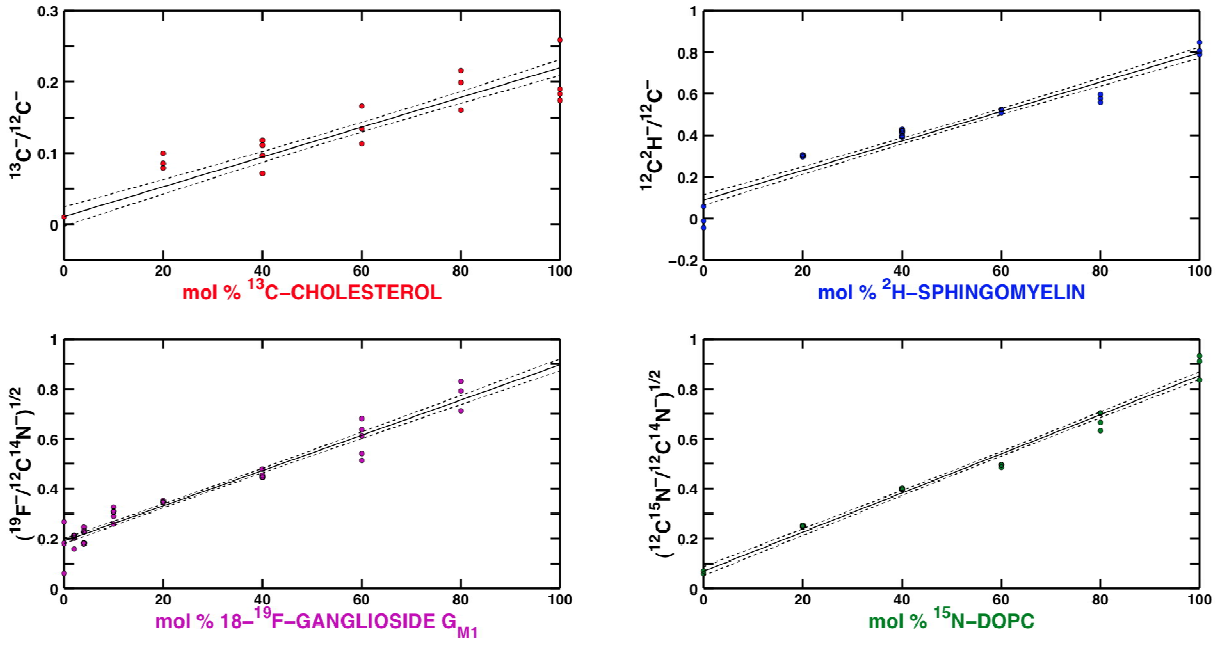

Figure S7. Dose-Response calibration curves from standard samples. Data points (circles) represent single nanoSIMS measurements (i.e. response) as a function of composition (i.e. dose). Solid lines represent the best-fit line for $r = mx + b$ (i.e. ^{13}C-Cholesterol and ^{2}H-Sphingomyelin) or $R = mx + b$ (i.e 18-^{19}F-Ganglioside G_{M1} and ^{15}N-DOPC). Upper and lower dashed lines represent upper and lower regression bands (see **Table S1** for best-fit line parameters and **Table S2** for the sensitivity and detection limits for these calibration curves).

Table S1. Best-fit line parameters for Calibration Curves in Figure S5.

r = mx + b* or *R = mx + b	**^{13}C-Cholesterol**	**^{12}H-Sphingomyelin**	**18-^{19}F-Ganglioside G_{M1}**	**^{15}N-DOPC**
m	0.00209	0.00709	0.00707	0.00784
b	0.0110	0.0888	0.190	0.0694

Table S2. Sensitivity and detection limits for Calibration Curves in Figure S5.

	^{13}C-Cholesterol	**^{12}H-Sphingomyelin**	**18-^{19}F-Ganglioside G_{M1}**	**^{15}N-DOPC**
Sensitivity	0.0138	0.0276	0.0160	0.0186
Detection limit [mol %]	12	6	2	4

Error Analysis

A	counts for species A
B	counts for species B
dA	uncertainty in counts of species A from Poisson counting statistics
dB	uncertainty in counts of species B from Poisson counting statistics
r	ratio of A to B
dr	uncertainty in ratio from propagating uncertainties in A and B in quadrature

For a linear calibration curve

$r = mx + b$	represents best fit line for the ratio vs mol% calibration curve, where m is the slope of the line and b is the y-intercept.
S_x	uncertainty in x from best-fit line
σ_r	standard deviation in r from best-fit line
n	number of standard sample measurements
k	number of replicate measurements for r
r^+ *and* r^-	upper and lower regression bands
dx^+ *and* dx^-	upper and lower sum of uncertainties in mol% from dr and S_x

For a quadratic calibration curve

$R = r^{1/2}$	represents the square root of the ratio
$R = mx + b$	represents best fit line for the square root of the ratio vs mol% calibration curve, where m is the slope of the line and
S_x	uncertainty in mol% from best-fit line
σ_R	standard deviation in r from best-fit line
n	number of standard sample measurements
k	number of replicate measurements for r
R^+ and R^-	upper and lower regression lines from best fit-line
dx^+ and dx^-	upper and lower sum of uncertainties in mol% from dr and S_x

Determining the error in composition based on a linear calibration curve

A

B

$dA = \sqrt{A}$

$dB = \sqrt{B}$

$$r = \frac{A}{B}$$

$$(dr)^2 = \left(\frac{\partial r}{\partial A} dA\right)^2 + \left(\frac{\partial r}{\partial B} dB\right)^2$$

$$dr = r\left[\left(\frac{1}{\sqrt{A}}\right)^2 + \left(\frac{1}{\sqrt{B}}\right)^2\right]^{1/2}$$

$$r = mx + b$$

$$S_x = \frac{\sigma_r}{m}\left[\frac{1}{n} + \frac{1}{k} + \frac{(r - \bar{r})^2}{m^2 \sum_{i=1}^{n} (x_i - \bar{x})^2}\right]^{1/2}$$

$$\sigma_r = \left[\sum_{i=1}^{n} \frac{(r_i - mx_i - b)^2}{n - 2}\right]^{1/2}$$

$$r^+ = m(x + S_x) + b$$

$$r^- = m(x - S_x) + b$$

$$dx^+ = \frac{dr}{m} + \frac{\sigma_r}{m}\left[\frac{1}{n} + \frac{1}{k} + \frac{(r + dr - \bar{r})^2}{m^2 \sum_{i=1}^{n} (x_i - \bar{x})^2}\right]^{1/2}$$

$$dx^- = \frac{dr}{m} + \frac{\sigma_r}{m}\left[\frac{1}{n} + \frac{1}{k} + \frac{(r - dr - \bar{r})^2}{m^2 \sum_{i=1}^{n} (x_i - \bar{x})^2}\right]^{1/2}$$

Determining the error in composition based on a quadratic calibration curve

A

B

$dA = \sqrt{A}$

$dB = \sqrt{B}$

$$R = \sqrt{r} = \sqrt{\frac{A}{B}}$$

$$(dR)^2 = \left(\frac{\partial R}{\partial A}\,dA\right)^2 + \left(\frac{\partial R}{\partial B}\,dB\right)^2$$

$$dR = \frac{R}{2}\left[\left(\frac{1}{\sqrt{A}}\right)^2 + \left(\frac{1}{\sqrt{B}}\right)^2\right]^{1/2}$$

$$R = mx + b$$

$$S_x = \frac{\sigma_R}{m}\left[\frac{1}{n} + \frac{1}{k} + \frac{(R-\bar{R})^2}{m^2\sum_{i=1}^{n}(x_i - \bar{x})^2}\right]^{1/2}$$

$$\sigma_r = \left[\sum_{i=1}^{n}\frac{(R_i - mx_i - b)^2}{n-2}\right]^{1/2}$$

$$R^+ = m(x + S_x) + b$$

$$R^- = m(x - S_x) + b$$

$$dx^+ = \frac{dR}{m} + \frac{\sigma_R}{m}\left[\frac{1}{n} + \frac{1}{k} + \frac{(R+dR-\bar{r})^2}{m^2\sum_{i=1}^{n}(x_i - \bar{x})^2}\right]^{1/2}$$

$$dx^- = \frac{dR}{m} + \frac{\sigma_R}{m}\left[\frac{1}{n} + \frac{1}{k} + \frac{(R-dR-\bar{r})^2}{m^2\sum_{i=1}^{n}(x_i - \bar{x})^2}\right]^{1/2}$$

Determining the error in the normalized composition.

x_i mol % for component i

dx_i uncertainty in mol % for component i

X_i Normalized mol % for component i

dX_i Uncertainty in normalized mol % for component i

n Total number of components (i.e. n = 4)

$$X_i = \frac{x_i}{\sum_{i=1}^{n} x_i} \times 100$$

$$dX_i = X_i \left[\left(\frac{dx_i}{x_i} \right)^2 + \left[\frac{\left(\sum_{i=1}^{n} (dx_i)^2 \right)^{1/2}}{\sum_{i=1}^{n} x_i} \right]^2 \right]^{1/2}$$

Quantitative Analysis

Micrometer Scale Phases

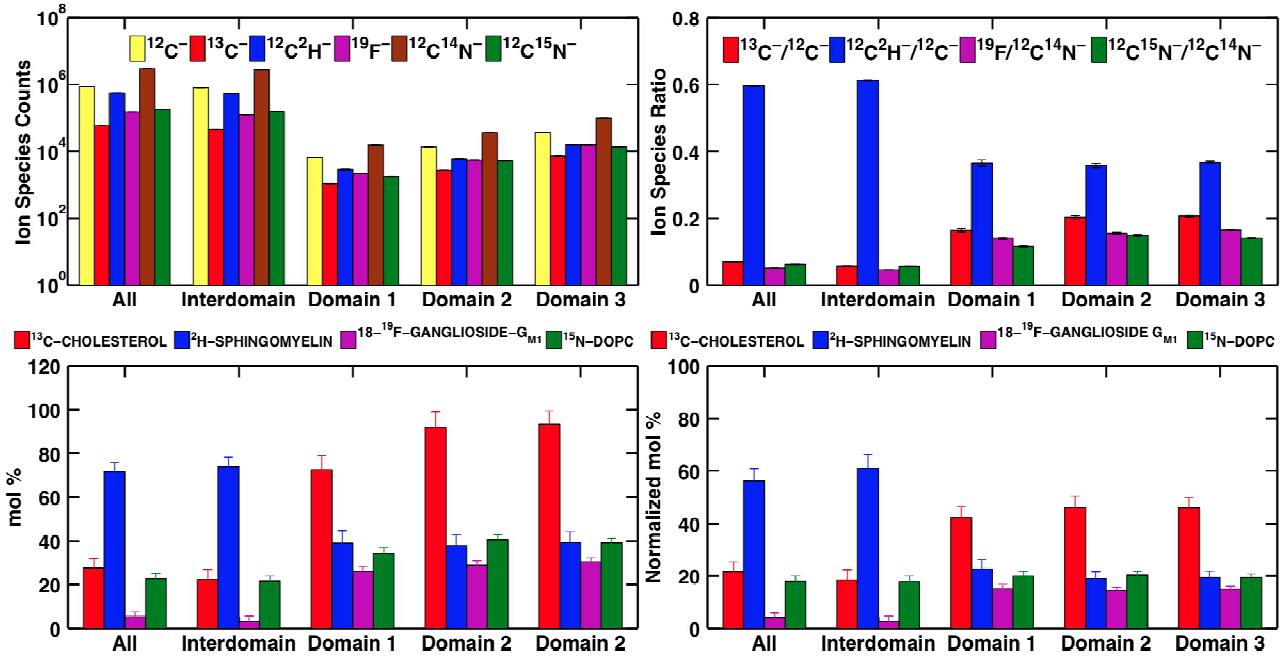

Figure S8. Ion species counts ($A \pm \sqrt{A}$), ion species ratio ($r \pm dr$), mol % ($x \pm dx$), and normalized mol% ($X \pm dX$) for the micrometer-scale phases.

Included Nanometer-scale Domains

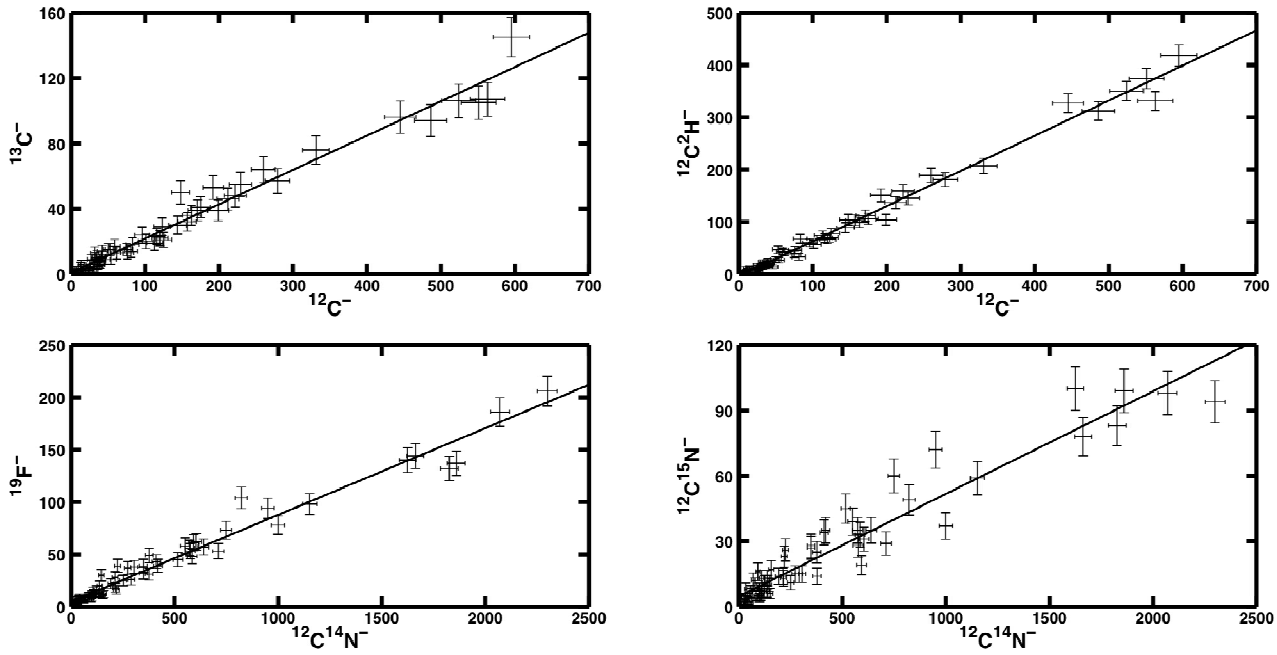

Figure S9. Data points represent ion species A (A ± √A) vs ion species B (B±√B) for the included, nanometer-scale domains (total of 68 domains). Solid lines represent the best-fit line $y = rx + c$, where r is the slope of the line (i.e. the ratio of A to B) and c the y-intercept (see Table S3 for best-fit line parameters).

Table S3. Best-fit line parameters from Figure S7.

y = rx + c	$^{13}C^-$ v $^{12}C^-$ Cholesterol	$^{12}C^2H^-$ v $^{12}C^-$ Sphingomyelin	$^{19}F^-$ v $^{12}C^{14}N^-$ Ganglioside G_{M1}	$^{12}C^{15}N^-$ v $^{12}C^{14}N^-$ DOPC
$r \pm dr$	0.210 ± 0.00427	0.672 ± 0.00885	0.829 ± 0.00179	0.0471 ± 0.00171
$c \pm dc$	0.825 ± 0.814	-4.15 ± 1.69	4.85 ± 1.21	4.67 ± 1.16

Excluded Nanometer-scale Domains

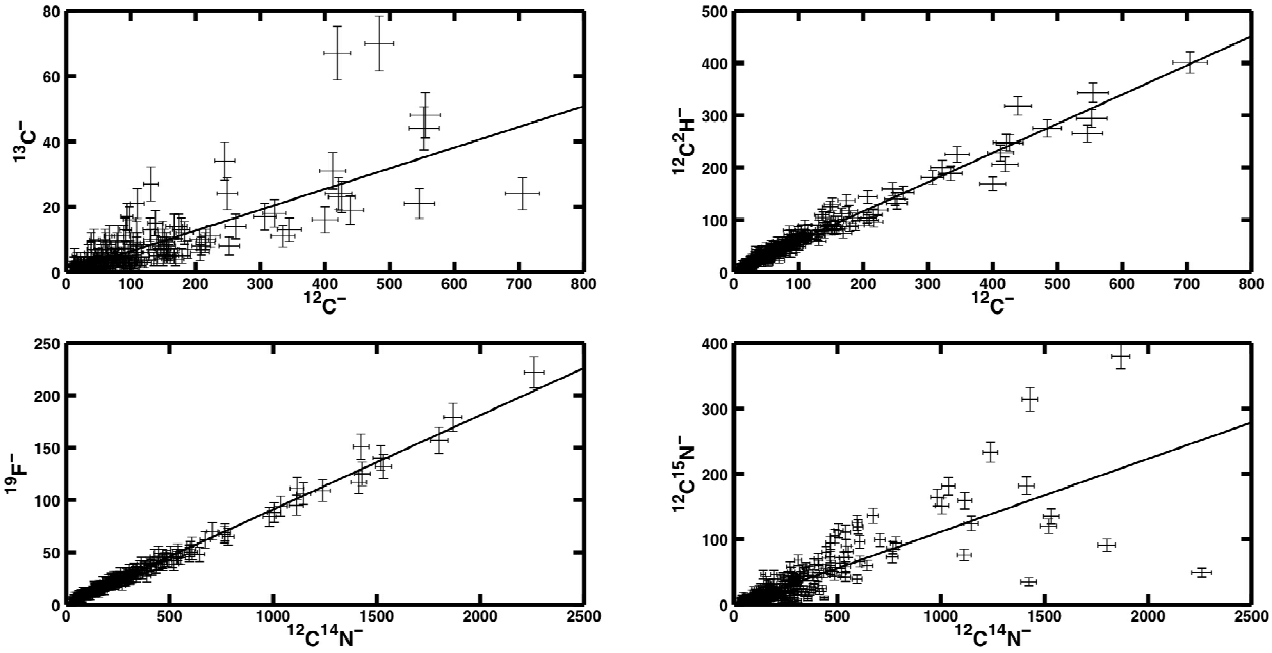

Figure S10. Data points represent ion species A (A ± √A) vs ion species B (B±√B) from the excluded, nanometer-scale domains (total of 318 domains). Solid lines represent the best-fit line $y = rx + c$, where r is the slope of the line (i.e. the ratio of A to B) and c the y-intercept (see Table S5 for best-fit line parameters).

Table S4. Best-fit line parameters from Figure S7.

y = rx + c	$^{13}C^-$ v $^{12}C^-$ Cholesterol	$^{12}C^2H^-$ v $^{12}C^-$ Sphingomyelin	$^{19}F^-$ v $^{12}C^{14}N^-$ Ganglioside G_{M1}	$^{12}C^{15}N^-$ v $^{12}C^{14}N^-$ DOPC
$r \pm dr$	0.0635 ± 0.00283	0.558 ± 0.00654	0.0901 ± 0.000603	0.111 ± 0.00464
$c \pm dc$	0.0124 ± 0.362	4.80 ± 0.839	0.949 ± 0.240	0.0159 ± 1.85

Peripheral Nanometer-scale Domains

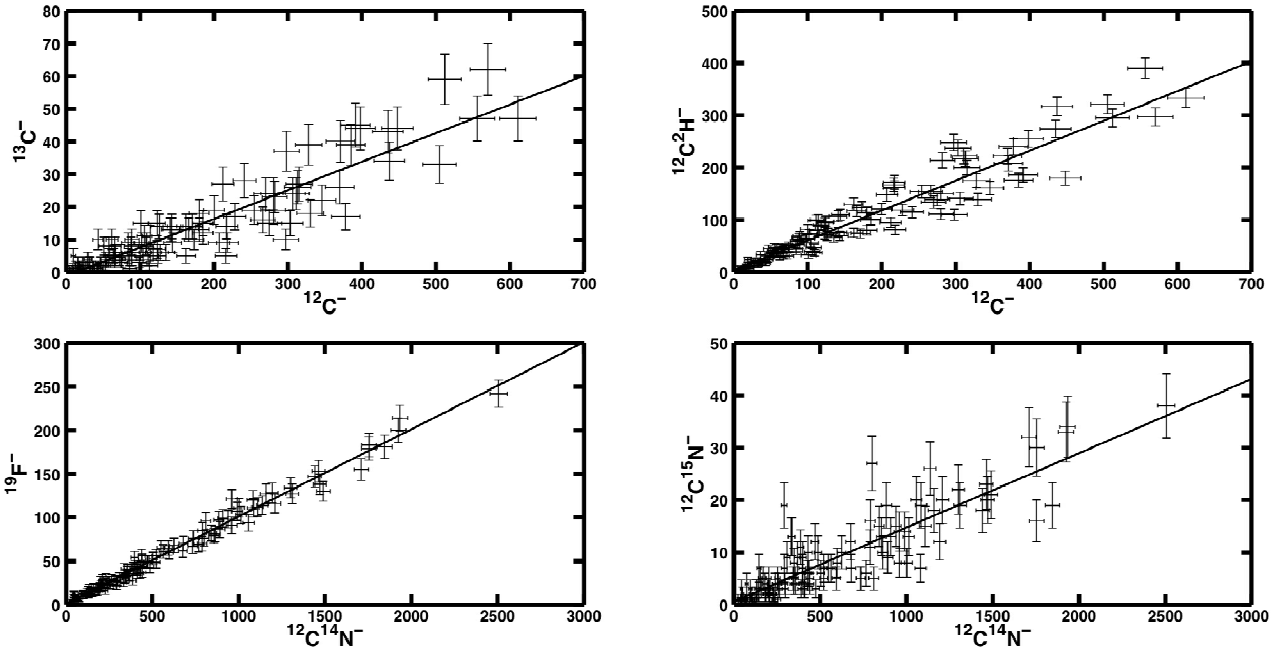

Figure S11. Data points represent ion species A (A ± √A) vs ion species B (B±√B) from the peripheral, nanometer-scale domains (total of 125 domains). Solid lines represent the best-fit line $y = rx + c$, where r is the slope of the line (i.e. the ratio of A to B) and c the y-intercept (see Table S4 for best-fit line parameters).

Table S5. Best-fit line parameters from Figure S7.

y = rx + c	$^{13}C^-$ v $^{12}C^-$ Cholesterol	$^{12}C^2H^-$ v $^{12}C^-$ Sphingomyelin	$^{19}F^-$ v $^{12}C^{14}N^-$ Ganglioside G_{M1}	$^{12}C^{15}N^-$ v $^{12}C^{14}N^-$ DOPC
$r \pm dr$	0.0875 ± 0.00338	0.571 ± 0.0162	0.100 ± 0.00114	0.0142 ± 0.000669
$c \pm dc$	-1.19 ± 0.722	3.81 ± 3.45	1.04 ± 0.865	0.565 ± 0.508

Summarized compositional analysis for the included, excluded and peripheral nanometer-scale phases.

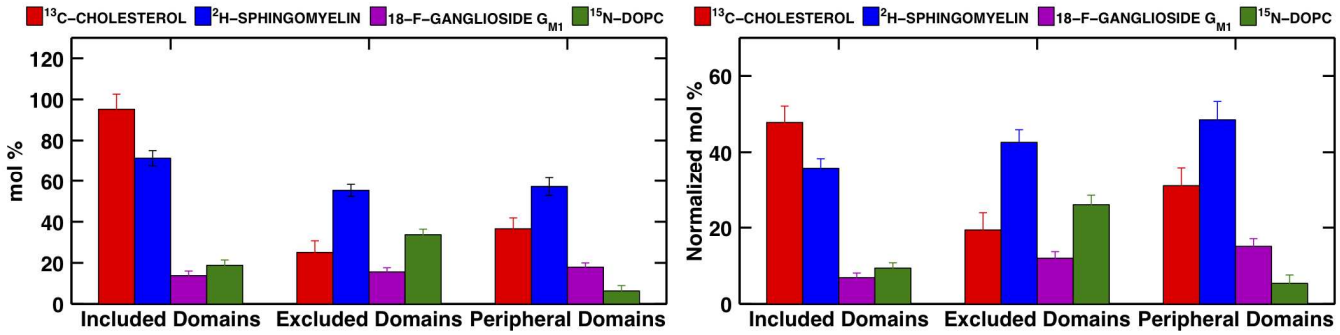

Figure S12. Calculated molar percentages ($x \pm dx$) from calibration curves and normalized molar percentages ($X \pm dX$).

NanoSIMS Imaging and Quantitative Compositional Analysis of Additional GUV Lipid Bilayers

Table S6. Compositional analysis of a GUV lipid bilayer population (total of 11 GUV lipid bilayers).

GUV #	Area [μm^2]	mol% Cholesterol	mol% PSM	mol% G_{M1}	mol% DOPC
1 (**Figure S13**)	1333.6	27.4 ± 4.1	51.5 ± 3.3	1.6 ± 2.0	19.5 ± 2.4
2 (**Figure S16**)	948.9	28.1 ± 2.6	53.2 ± 2.7	5.6 ± 1.4	13.1 ± 1.7
3 (**Figure 2**)	746.6	21.7 ± 3.6	56.2 ± 3.3	4.2 ± 1.7	17.9 ± 2.0
4 (**Figure S19**)	637.2	26.6 ± 3.9	46.6 ± 2.9	8.4 ± 1.9	18.4 ± 2.3
5 (**Figure S22**)	527.2	23.8 ± 3.5	45.2 ± 2.7	14.6 ± 1.7	16.4 ± 2.0
6	523.1	26.1 ± 3.5	33.1 ± 2.2	25.9 ± 1.7	15.0 ± 2.0
7	279.7	21.2 ± 4.8	24.1 ± 2.9	37.4 ± 2.6	17.3 ± 2.6
8	265.8	17.6 ± 5.8	61.3 ± 4.9	6.3 ± 2.4	14.8 ± 2.9
9	258.5	17.1 ± 5.5	57.7 ± 4.5	8.3 ± 2.3	16.9 ± 2.8
10	178.9	20.9 ± 6.2	42.7 ± 4.2	19.5 ± 2.7	16.9 ± 3.1
11	159.6	28.2 ± 3.4	27.7 ± 2.2	19.9 ± 1.6	24.2 ± 2.0
Average ± Std. Dev		23.5 ± 4.1	45.4 ± 12.4	13.8 ± 10.9	17.3 ± 2.9

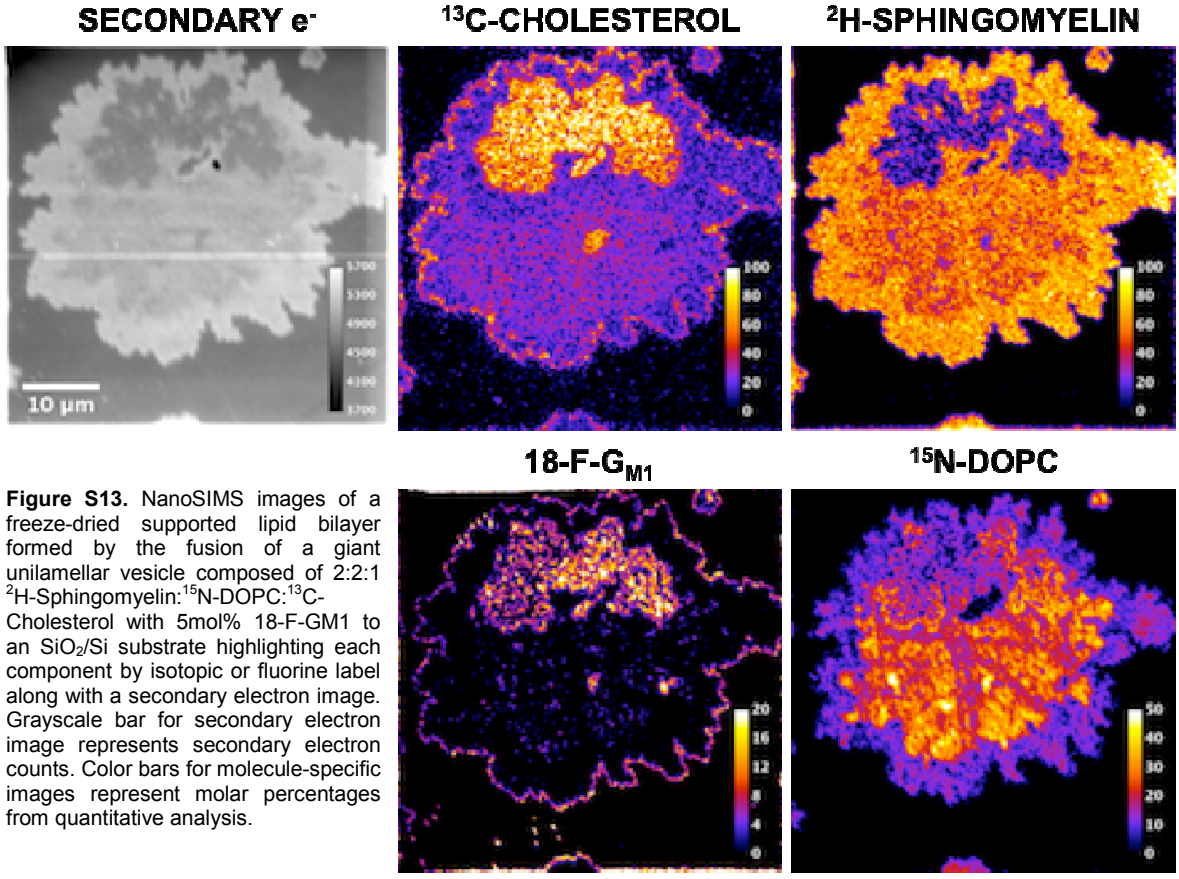

Figure S13. NanoSIMS images of a freeze-dried supported lipid bilayer formed by the fusion of a giant unilamellar vesicle composed of 2:2:1 ^{2}H-Sphingomyelin:^{15}N-DOPC:^{13}C-Cholesterol with 5mol% 18-F-GM1 to an SiO_2/Si substrate highlighting each component by isotopic or fluorine label along with a secondary electron image. Grayscale bar for secondary electron image represents secondary electron counts. Color bars for molecule-specific images represent molar percentages from quantitative analysis.

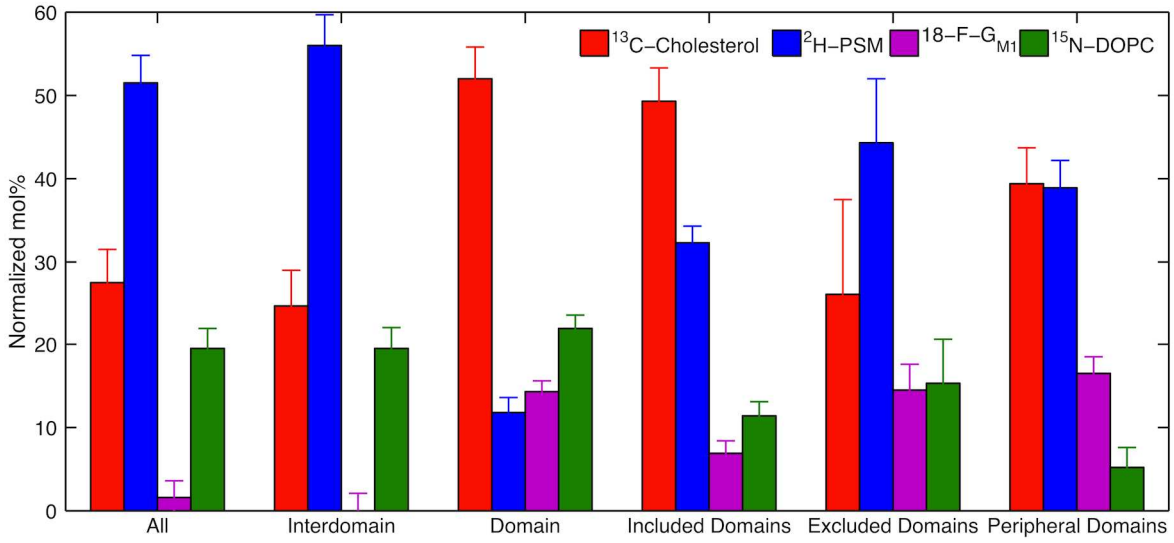

Figure S14. Quantitative compositional analysis of **Figure S13** for the entire lipid bilayer (All); the interdomain region (Interdomain); the micrometer-scale domain; and, the nanometer-scale domains localized within the micrometer scale domains, the interdomain region and the edge of the lipid bilayer referred to as Included, Excluded, and Peripheral Domains, respectively.

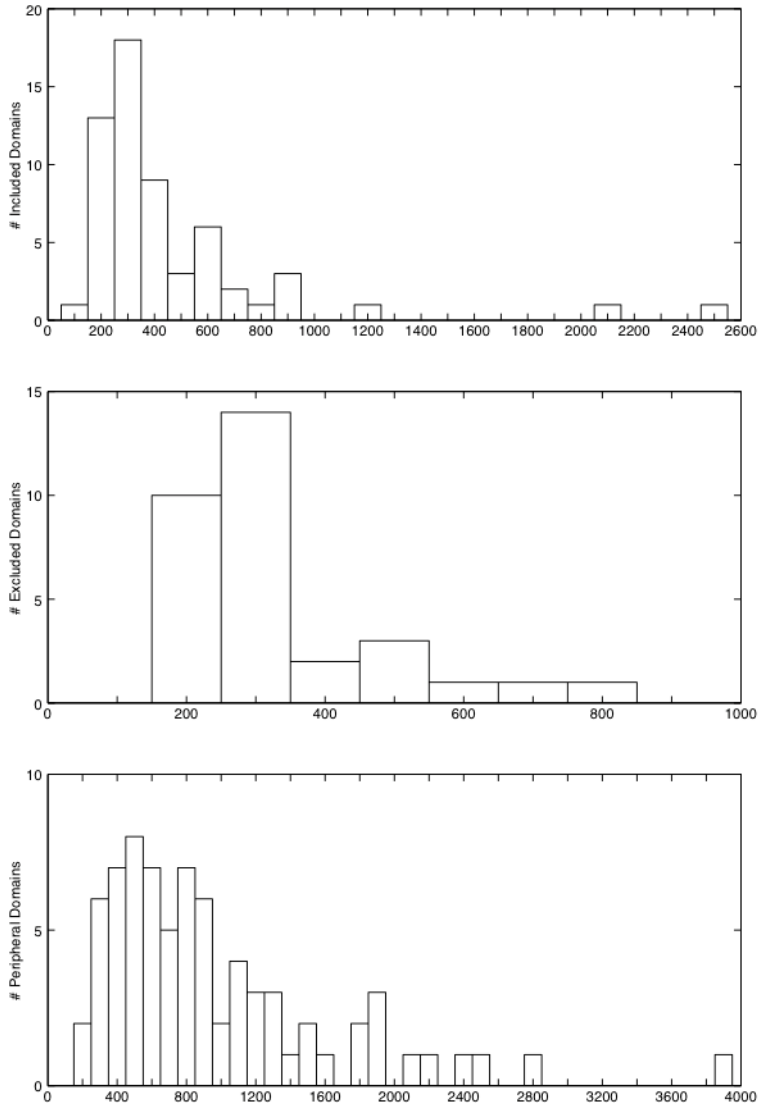

Figure S15. Size distribution analysis for **Figure S13** of the nanometer-scale domains localized within the micrometer-scale domains, the interdomain region and the edge of the lipid bilayer referred to as included, excluded, and peripheral domains, respectively.

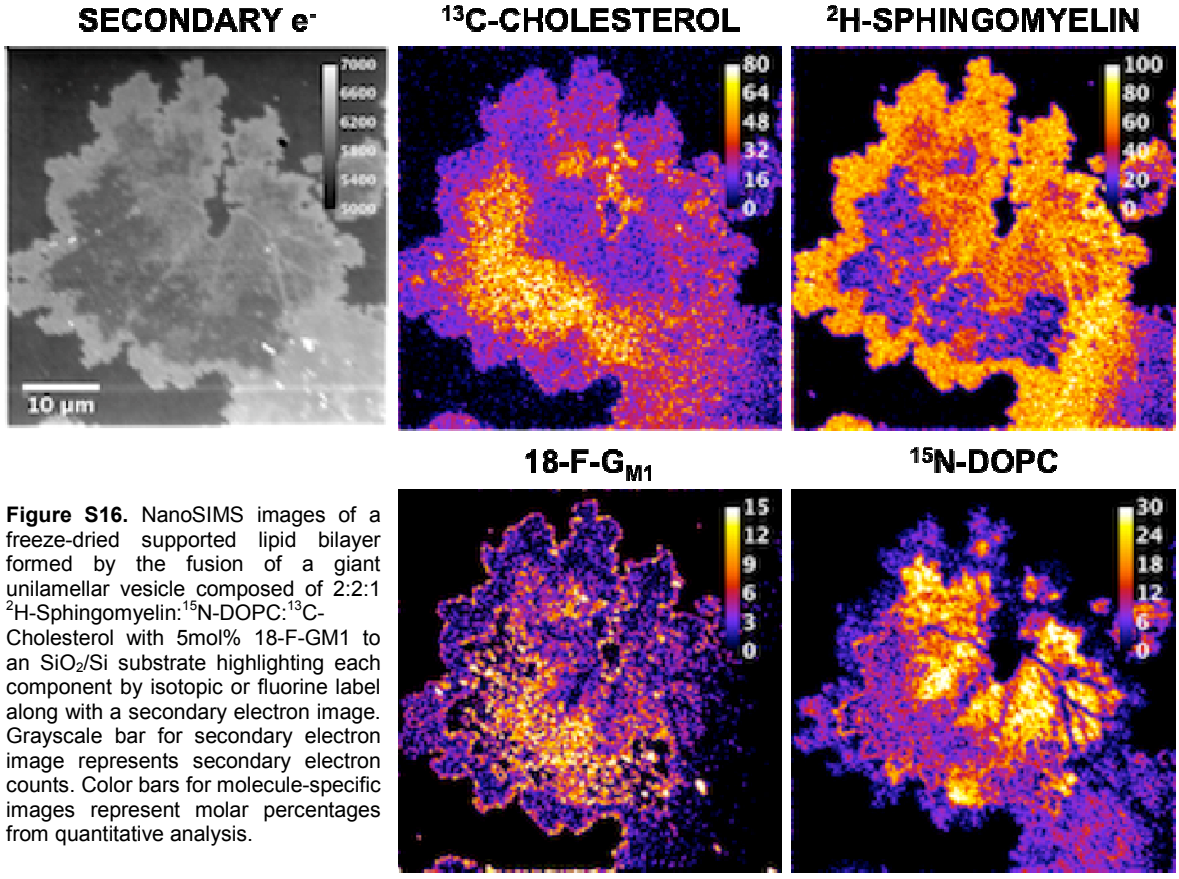

Figure S16. NanoSIMS images of a freeze-dried supported lipid bilayer formed by the fusion of a giant unilamellar vesicle composed of 2:2:1 ^{2}H-Sphingomyelin:^{15}N-DOPC:^{13}C-Cholesterol with 5mol% 18-F-GM1 to an SiO_2/Si substrate highlighting each component by isotopic or fluorine label along with a secondary electron image. Grayscale bar for secondary electron image represents secondary electron counts. Color bars for molecule-specific images represent molar percentages from quantitative analysis.

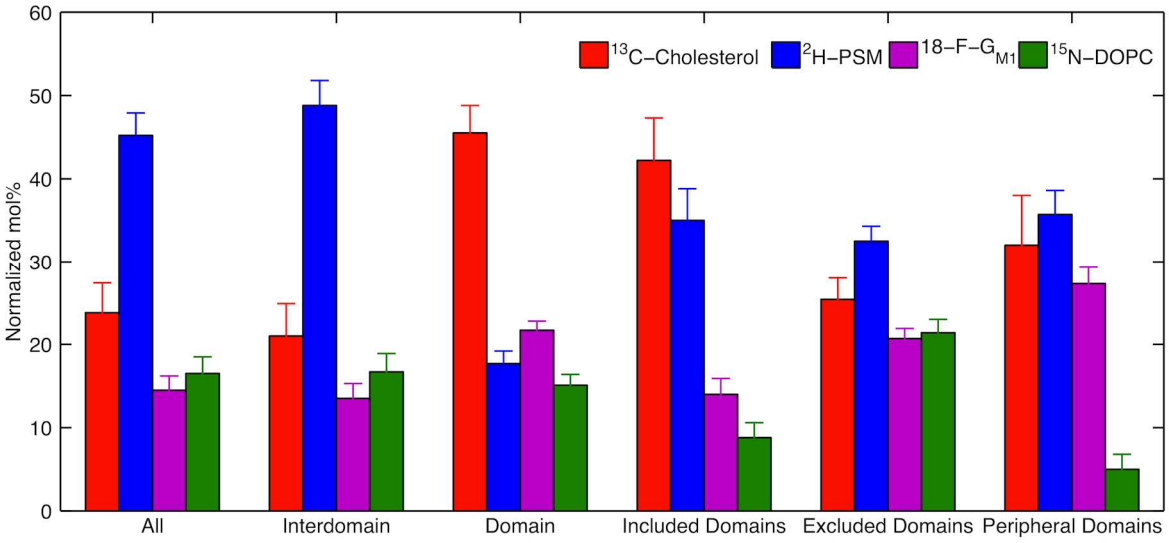

Figure S17. Quantitative compositional analysis of **Figure S16** for the entire lipid bilayer (All); the interdomain region (Interdomain); the micrometer-scale domain; and, the nanometer-scale domains localized within the micrometer scale domains, the interdomain region and the edge of the lipid bilayer referred to as Included, Excluded, and Peripheral Domains, respectively.

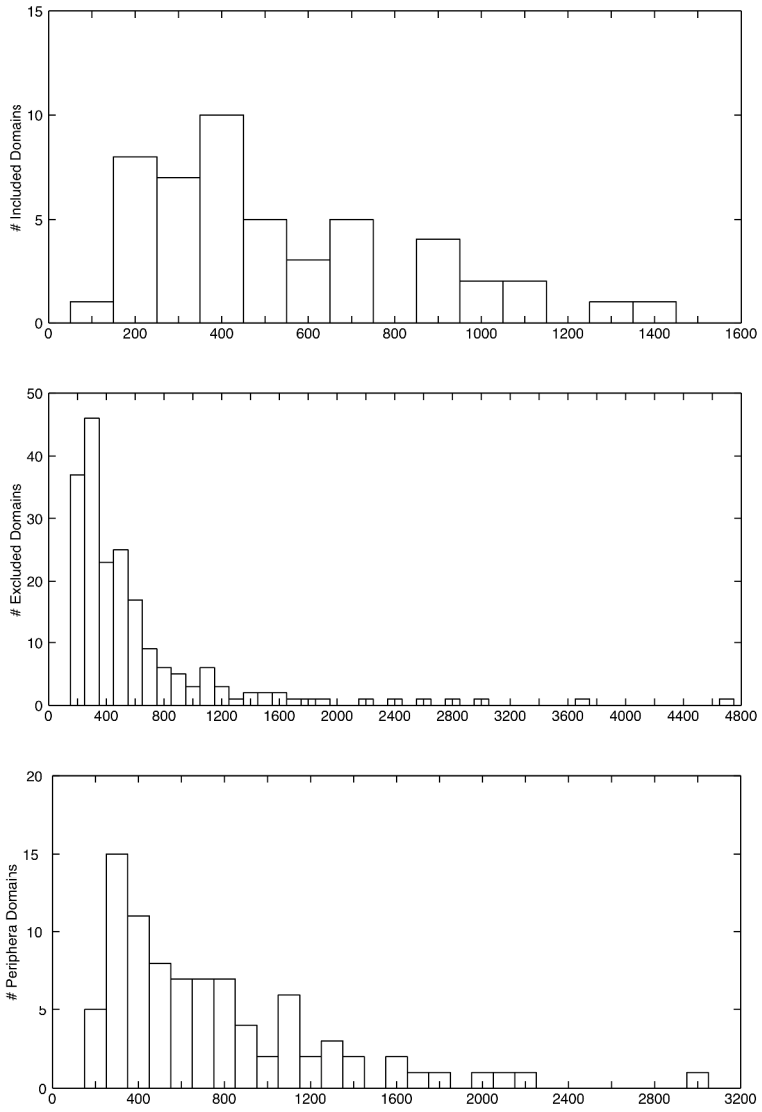

Figure S18. Size distribution analysis for **Figure S16** of the nanometer-scale domains localized within the micrometer-scale domains, the interdomain region and the edge of the lipid bilayer referred to as included, excluded, and peripheral domains, respectively.

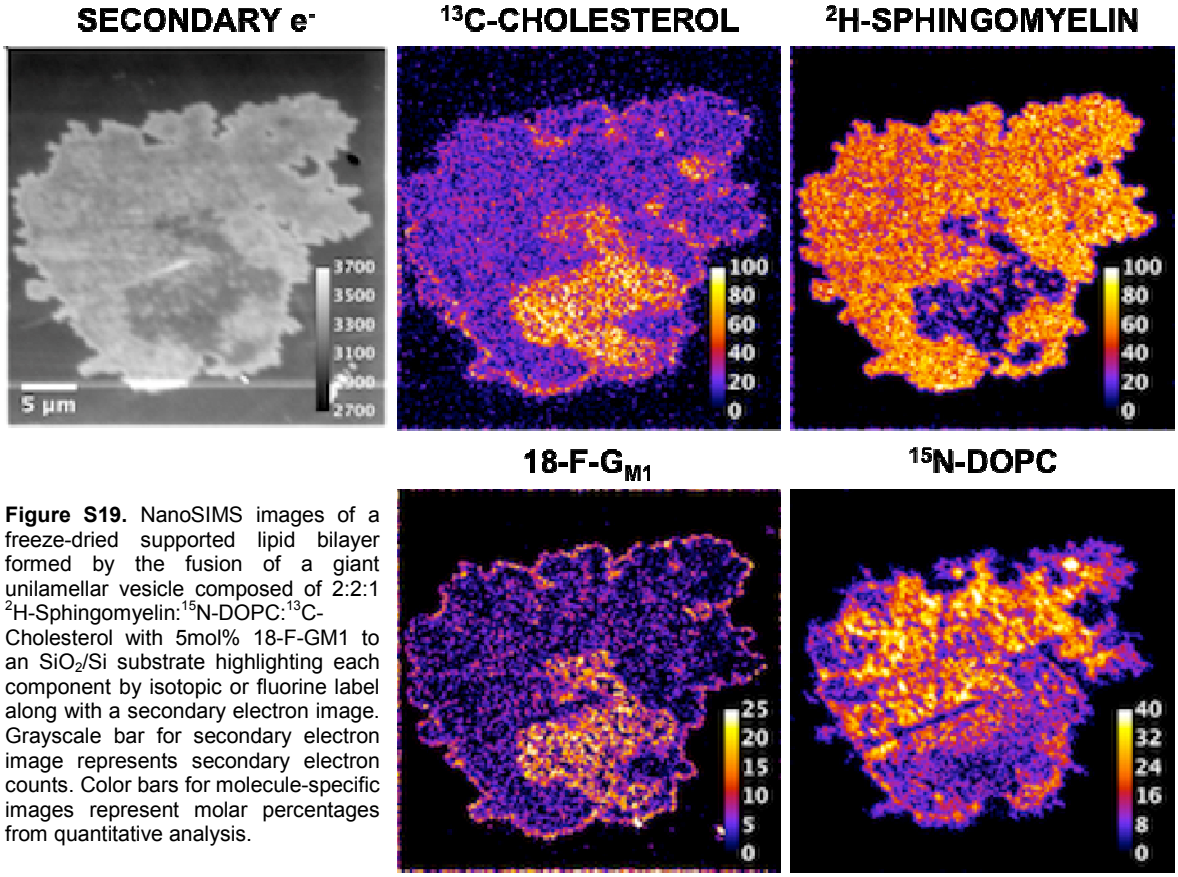

Figure S19. NanoSIMS images of a freeze-dried supported lipid bilayer formed by the fusion of a giant unilamellar vesicle composed of 2:2:1 ^{2}H-Sphingomyelin:^{15}N-DOPC:^{13}C-Cholesterol with 5mol% 18-F-GM1 to an SiO_2/Si substrate highlighting each component by isotopic or fluorine label along with a secondary electron image. Grayscale bar for secondary electron image represents secondary electron counts. Color bars for molecule-specific images represent molar percentages from quantitative analysis.

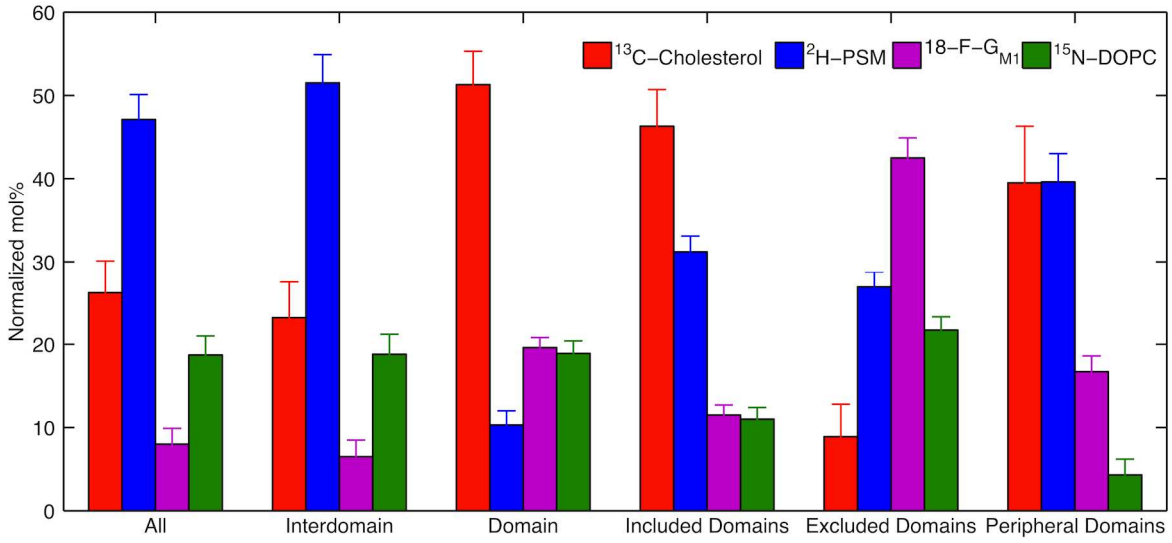

Figure S20. Quantitative compositional analysis of **Figure S19** for the entire lipid bilayer (All); the interdomain region (Interdomain); the micrometer-scale domain; and, the nanometer-scale domains localized within the micrometer scale domains, the interdomain region and the edge of the lipid bilayer referred to as Included, Excluded, and Peripheral Domains, respectively.

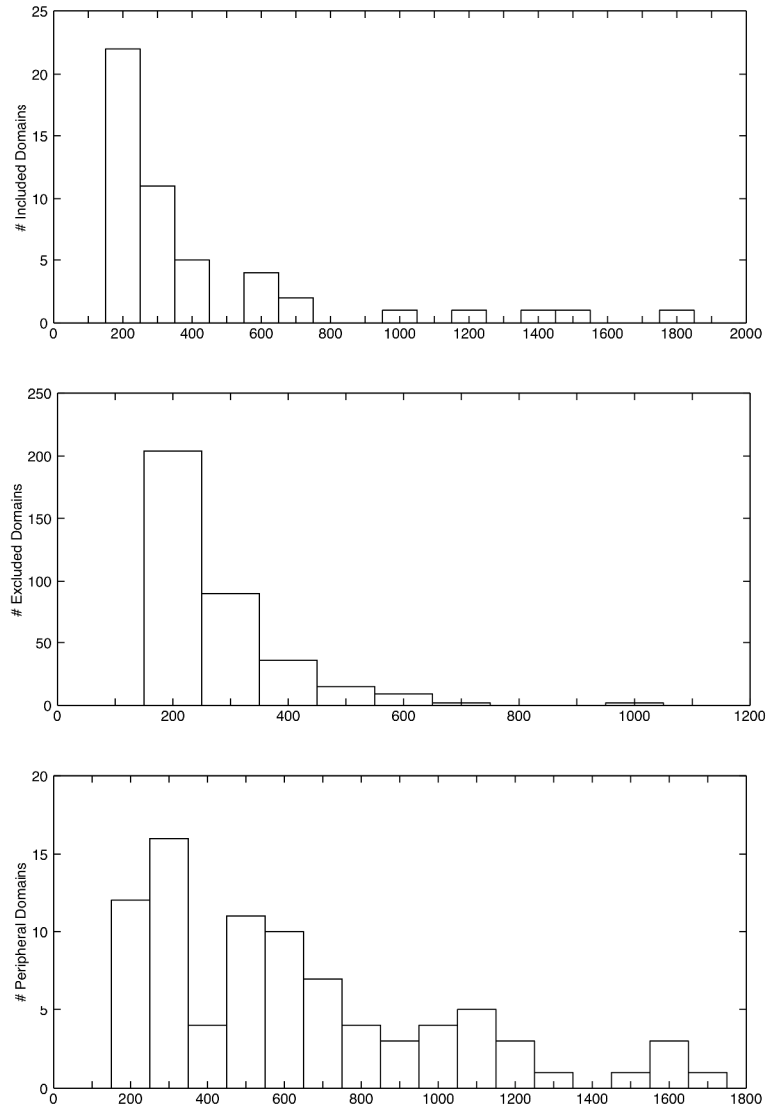

Figure S21. Size distribution analysis for **Figure S19** of the nanometer-scale domains localized within the micrometer-scale domains, the interdomain region and the edge of the lipid bilayer referred to as included, excluded, and peripheral domains, respectively.

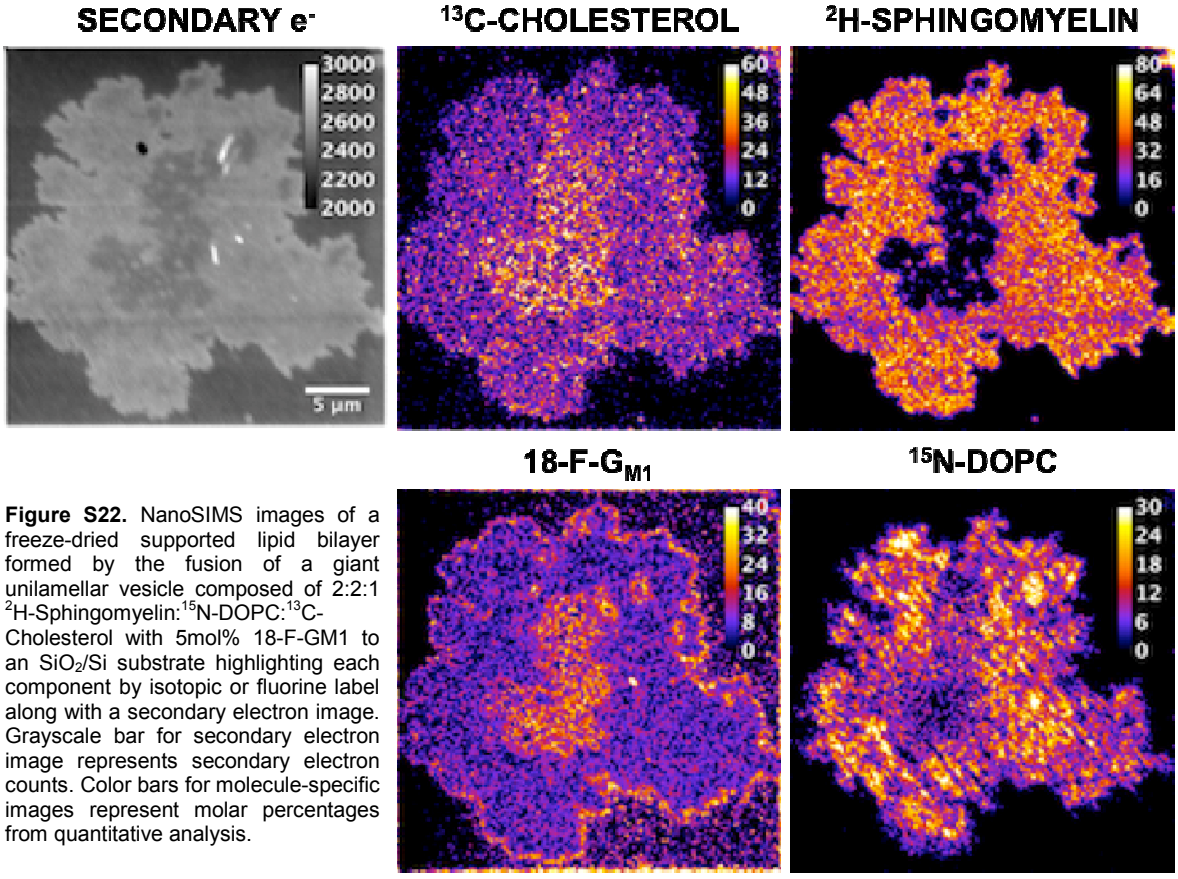

Figure S22. NanoSIMS images of a freeze-dried supported lipid bilayer formed by the fusion of a giant unilamellar vesicle composed of 2:2:1 ^{2}H-Sphingomyelin:^{15}N-DOPC:^{13}C-Cholesterol with 5mol% 18-F-GM1 to an SiO_2/Si substrate highlighting each component by isotopic or fluorine label along with a secondary electron image. Grayscale bar for secondary electron image represents secondary electron counts. Color bars for molecule-specific images represent molar percentages from quantitative analysis.

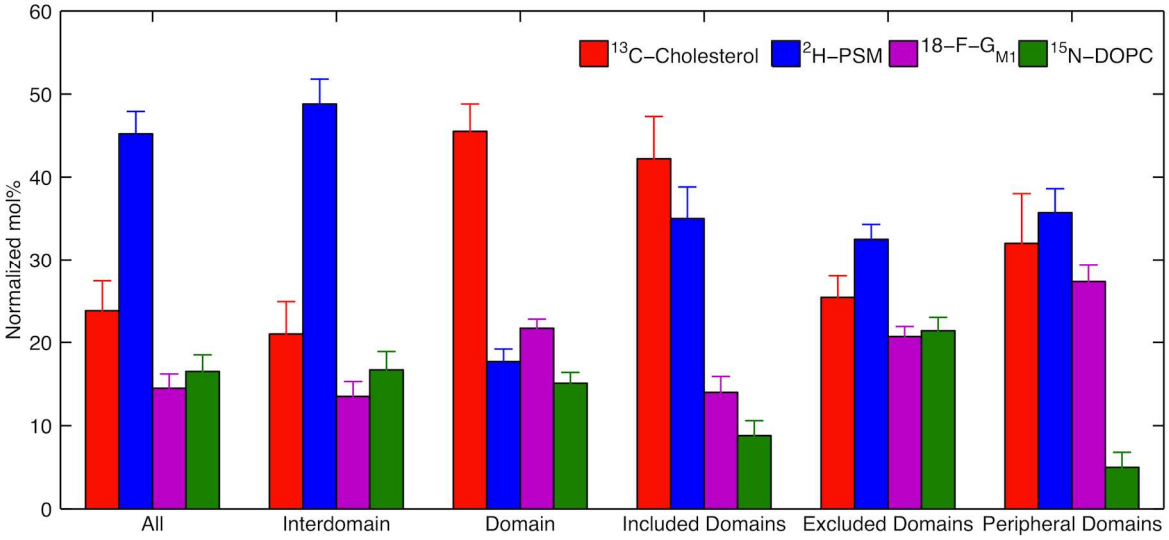

Figure S23. Quantitative compositional analysis of **Figure S22** for the entire lipid bilayer (All); the interdomain region (Interdomain); the micrometer-scale domain; and, the nanometer-scale domains localized within the micrometer scale domains, the interdomain region and the edge of the lipid bilayer referred to as Included, Excluded, and Peripheral Domains, respectively.

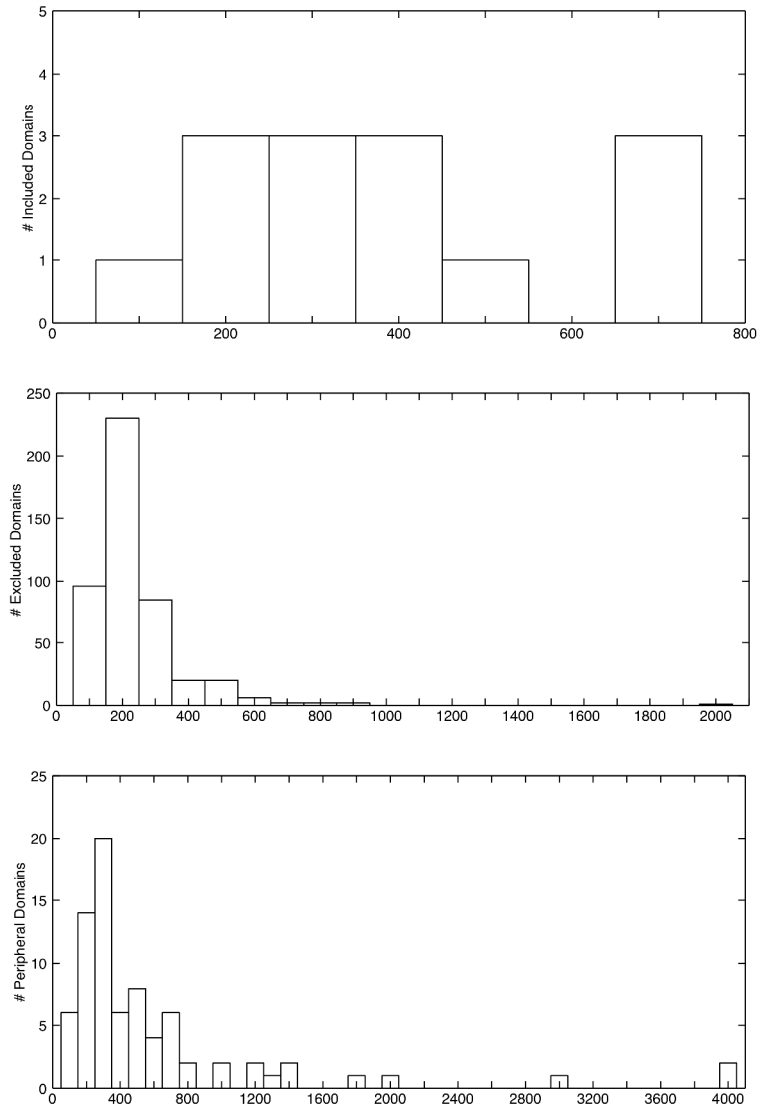

Figure S24. Size distribution analysis for **Figure S22** of the nanometer-scale domains localized within the micrometer-scale domains, the interdomain region and the edge of the lipid bilayer referred to as included, excluded, and peripheral domains, respectively.

Table S7. Summarized compositional analysis (Avg. ± Std. Dev.) for the different phases observed in Figures S13, S16, 2, S19 and S22

Phase	mol% Cholesterol	mol% PSM	mol% G_{M1}	mol% DOPC
Interdomain	22.4 ± 2.8	55.3 ± 5.1	5.3 ± 5.1	16.9 ± 3.0
Domains	46.6 ± 3.8	17.8 ± 5.1	16.4 ± 3.0	19.3 ± 2.1
Included Domains	44.0 ± 4.3	37.2 ± 6.9	9.1 ± 3.5	9.6 ± 1.5
Excluded Domains	20.7 ± 7.4	38.8 ± 8.7	19.9 ± 13.3	20.7 ± 3.2
Peripheral Domains	33.8 ± 5.4	43.9 ± 8.3	17.5 ± 5.7	4.8 ± 0.5

Imaging the lateral distribution of fluorinated G_{M1} analogues within phase separated lipid bilayers

In these studies we additionally tested the lateral distribution of another monofluorinated G_{M1} analogue within phase separated lipid bilayers. The difference between the monofluorinated G_{M1} discussed in the main manuscript and the one discussed here in the supporting information is the position of the ^{19}F-atom along the fatty acid residue, either at position 18 or 12, respectively. The position 12,^{19}F-Ganglioside G_{M1} (12-F-G_{M1}, Figure S17) analogue displayed a phase behavior that was significantly different. Two main regions were resolved corresponding to: 1) a micrometer-scale, G_{M1}/Cholesterol-rich, liquid-ordered domain phase and 2) a surrounding, PSM/DOPC-rich, liquid-disordered interdomain region.

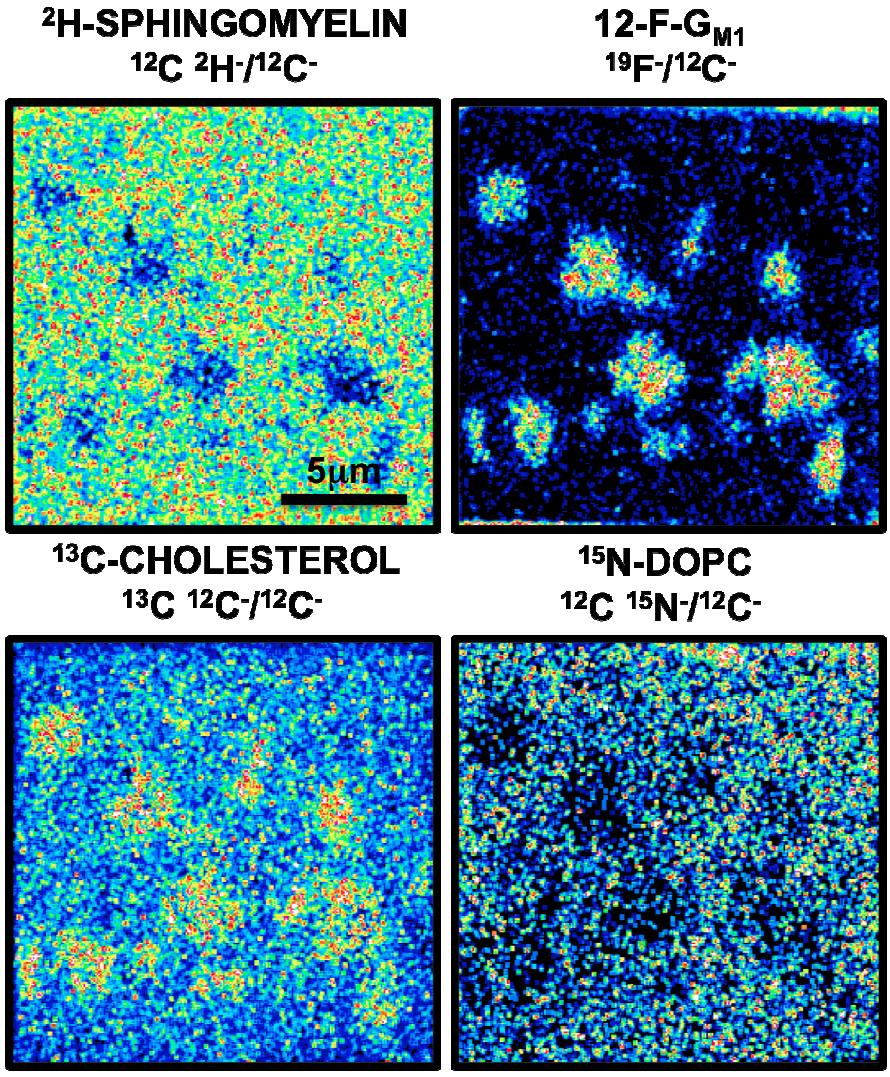

Figure S21. NanoSIMS images of 12-F-G_{M1}-containing lipid bilayers. The lateral distribution of the monofluorinated (19F-atom in position 12 along the fatty acid residue) ganglioside GM1 into PSM-poor/Cholesterol-rich/DOPC-poor micrometer-scale domains.

References

1. Rothblat, G. H.; Arbogast, L. Y.; Ouellette, L.; Howard, B. V., Preparation of De-Lipidized Serum-Protein for Use in Cell-Culture Systems. *In Vitro-Journal of the Tissue Culture Association* **1976,** 12, (8), 554-557.
2. Folch, J. J.; Lees, M. M.; Stanley, G. H. G. S. *J Biol Chem* **1957**, *226*, 497–509.
3. Suzuki, K. *J Neurochem* **1965**, *12*, 629–638.
4. Wersto, R. Methods in Cell Science **1982**.
5. Wersto, R. P.; Druyan, M. E., Microprocedure for the isolation and quantification of phospholipids from tissue culture derived cells. *Journal of Tissue Culture Methods* **1982,** 7, (4), 155-158.
6. Kraft, M. L.; Weber, P. K.; Longo, M. L.; Hutcheon, I. D.; Boxer, S. G., Phase separation of lipid membranes analyzed with high-resolution secondary ion mass spectrometry. *Science* **2006**, 313, (5795),1948-1951.
7. Gouy, H.; Deterre, P.; Debré, P.; Bismuth, G. *J. Immunol.* **1994**, *152*, 3271–3281.
8. Leonenko, Z. V.; Finot, E.; Ma, H.; Dahms, T. E. S.; Cramb, D. T. *Biophys. J.* **2004**, *86*, 3783–3793.